# Shell-Isolated Nanoparticle-Enhanced Raman Spectroscopy: Expanding the Versatility of Surface-Enhanced Raman Scattering

Jason R. Anema, Jian-Feng Li, Zhi-Lin Yang, Bin Ren, and Zhong-Qun Tian*

State Key Laboratory of Physical Chemistry of Solid Surfaces, Key Laboratory of Analytical Sciences and College of Chemistry and Chemical Engineering, Xiamen University, Xiamen 361005, China; email: zqtian@xmu.edu.cn

Annu. Rev. Anal. Chem. 2011. 4:129–50

First published online as a Review in Advance on March 3, 2011

The *Annual Review of Analytical Chemistry* is online at anchem.annualreviews.org

This article's doi: 10.1146/annurev.anchem.111808.073632



1936-1327/11/0719-0129$20.00

*Corresponding author.

## Keywords

core-shell nanoparticles, Au@silica, analytical chemistry, electrochemistry, surface chemistry, single crystals of Au(100), Au(111), Pt(111), and Rh(111)

## Abstract

Surface-enhanced Raman scattering (SERS) is a powerful technique for detection and characterization because of its extremely high sensitivity and the rich structural information that it can offer. However, most SERS substrates are composed of Au, Ag, or Cu, and a lack of substrate generality has greatly limited the breadth of the use of SERS. Recently, we have devised a method by which SERS can be obtained from virtually any surface. Au nanoparticles are coated with ultrathin silica shells. The Au core provides Raman signal enhancement; the silica shell prevents the core from coming into direct contact with probe/analyte molecules or the surface over which these particles are spread (i.e., prevents the contamination of the chemical system under study). In the present review, we expand upon previous discussion of the enhancement mechanism; procedures for the synthesis and characterization of our nanoparticles; and applications in surface chemistry, electrochemistry, and inspection.

# 1. INTRODUCTION

## 1.1. Ordinary Raman Scattering and Surface-Enhanced Raman Scattering

**SERS:** surface-enhanced Raman scattering

**LSPs:** localized surface plasmons

**Single crystal:** a fragment of material wherein the constituent atoms have only one repeating spatial arrangement (unit cell); a single crystal typically has well-defined and atomically flat faces

**Enhancement factor (EF):** the number of times that the intensity of Raman scattering from a molecule is increased because of the molecule's proximity to a nanostructured free-electron (or free-electron-like) metal

**SHINERS:** shell-isolated nanoparticle-enhanced Raman spectroscopy

In Raman spectroscopy (1–3), energy transfer occurs while a molecule scatters a photon. The outgoing photon may have less (Stokes shifted) or more (anti-Stokes shifted) energy than the incident photon, and this difference corresponds to a change in the molecule's vibrational state. Energy transfer from the photon to the molecule is more probable statistically, and the spectroscopy of Stokes-shifted light is usually employed.

The advantage that Raman spectroscopy offers over fluorescence, which is a much more commonly used technique in analytical chemistry, lies in the rich structural information that the former method can provide. Probe/analyte molecules cannot be characterized or even identified directly by fluorescence, and fluorescent tags or markers are normally combined with analyte receptors in sensing applications. The greatest disadvantage associated with Raman spectroscopy is its lack of sensitivity. A typical Raman scattering cross section is $10^{-29}$ cm$^2$, whereas a typical fluorescence cross section is $10^{-19}$ cm$^2$ (4). However, surface enhancement can significantly increase the intensity of Raman scattering from a molecule (4).

Surface-enhanced Raman scattering (SERS) may occur if the molecule is located in close proximity to a nanostructured free-electron metal such as Au, Ag, or Cu (4–22). When light of an appropriate wavelength is incident on a nanostructured material of this type, collective oscillations in electron density occur (23–27). These oscillations are known as surface plasmons (SPs): either localized surface plasmons (LSPs) or propagating surface plasmons. Such oscillations lead to narrow regions of enhanced electromagnetic field strength that decay exponentially with distance from the surface (25–27). The average Raman enhancement (from regions of greater field strength as well as from regions of weaker field strength) may be as high as six orders of magnitude for the group IB metals Au, Ag, and Cu (14–16, 28). SERS may also be obtained from the nanostructured free-electron-like metals Pt, Ru, Rh, Pd, Fe, Co, and Ni in group VIIIB (29, 30), and they yield average enhancements ranging from one to three orders of magnitude (31).

The possibility of using SERS in analytical chemistry is very attractive, as SERS can provide rich structural information with a sensitivity that is comparable to that of fluorescence. Ultralow detection limits, down to the single-molecule regime (32–37), are possible with SERS. There are two significant drawbacks to the commonplace application of SERS in analytical chemistry, however: a lack of substrate/molecule generality and a lack of measurement reproducibility.

The first limitation, a lack of generality, is intrinsic to the SERS phenomenon. As explained above, SERS substrates must be nanostructured (they are morphology-specific), and they must be composed of a free-electron metal or a free-electron-like metal (they are materials-specific) to support SP modes. The effect is limited to approximately ten elements and, even then, cannot be used to study the atomically flat single crystals that are of interest to the surface science community. Furthermore, certain probe/analyte molecules may be incompatible with certain SERS substrates with regard to sensitivity in single- or even several-molecule studies (probe/analyte specificity) if their cross sections are too small to yield a strong signal given the maximum possible enhancement factor (EF) offered by the substrate. We address and overcome this first limitation, the lack of substrate/molecule generality, with shell-isolated nanoparticle-enhanced Raman spectroscopy (SHINERS) (38, 39). Here, nanoparticles (NPs) with a Au core and a dielectric shell are spread over any surface (e.g., single crystals and foodstuffs, both of which the present work discusses). The Au core provides a large Raman signal enhancement, and the dielectric shell prevents the core from interacting with (i.e., contaminating) the system under study.

The second limitation stems from an inability to manage hot spots, where most of the signal is generated. The precision of a SERS measurement is typically ~15–20% relative standard deviation

(40, 41), but this has been reduced to a few percent for applications in analytical chemistry (18, 41). The continued development of nanofabrication techniques is essential for improving SERS-measurement reproducibility; however, progress in this area is insufficient for a complete solution because the coinage metals (i.e., Au, Ag, and Cu) have such low cohesive energies (42). When a coinage metal SERS substrate is heated during irradiation, surface atoms move about with more kinetic energy, and SERS intensity decreases as the nanostructure deteriorates. The approach that we take in SHINERS may offer a solution to this problem as well: A shell or coating can hold surface atoms in place and prevent the degradation of precisely fabricated coinage metal nanostructures.

**SHIN:** shell-isolated nanoparticle

In the subsections that follow, we introduce our SHINERS NPs within the broader context of core-shell NPs (Section 1.2) and then discuss the advantages of our SHINERS method over other Raman signal–enhancing methods (Section 1.3). We examine the mechanism of enhancement in Section 2 and provide a detailed description of the synthesis and characterization of our SHINERS NPs in Section 3. In Sections 4, 5, and 6, we review some exemplary applications in surface science, electrochemistry, and inspection. We return to the question of generality in Section 7.1, and we look to the future of this exciting new technique in Section 7.2.



## 1.2. Core-Shell Nanoparticles and Shell-Isolated Nanoparticle-Enhanced Raman Spectroscopy

In **Figure 1** we categorize some of the different NP types used for SERS. Only spheres are shown, but other shapes such as rods (43) and cubes (44) are possible as well. First, we distinguish between bare NPs and core-shell NPs. We then divide core-shell NPs into those with an ultrathin shell (< approximately 5 nm) and those with a thicker shell. NPs with a thick shell of silica normally contain markers, magnets, and/or other machinery used to perform a particular function or a particular set of functions (45–58). Here, the shell is used to hold the various components of the NP together and to protect the overall structure from physical and chemical damage. A thicker shell can encompass larger components, and pinhole-free synthesis is easier. NPs with a core of silica and a thick shell of Au or Ag are of interest because the SP resonance wavelength can be tuned by adjusting the core's diameter and the shell's thickness (59–62). We note that micrometer-sized silica particles have also been coated with Au or Ag and used for SERS (63, 64). Ultrathin-shell NPs may be used to obtain SERS from a molecule on the surface of a weakly enhancing or nonenhancing material. Here, first the material is deposited on a coinage metal NP, and then the probe/analyte molecule is added as an additional layer. Enhanced field strength extends from the core's surface to the shell's surface, and the shell in effect borrows SERS activity from the core. It is critical that the shell be ultrathin because this long-range effect becomes exponentially weaker with distance from the enhancing surface (i.e., the core's surface). We have used this strategy to obtain SERS from a variety of adsorbates on transition metal (TM) surfaces (31).

Our Au@silica SHINERS NPs expand on the borrowed SERS strategy just described, again taking advantage of the long-range electromagnetic field enhancement effect. However, the role played by the shell, the location of the probe/analyte molecule, and the way in which the NPs are used differ substantially in SHINERS compared with a Au@TM experiment. In SHINERS, the probe/analyte molecule is located on a bulk sample of the weakly enhancing or nonenhancing material, and shell-isolated nanoparticles (SHINs) are spread on top to generate the SERS signal. The isolating shell, which is made of an inert dielectric material, helps to maintain spectral integrity by preventing direct contact between the core and the system under study. In other words, the core may be considered a contaminant and the shell keeps the core from interacting chemically or electrically with any components of the system under study, thereby minimizing the

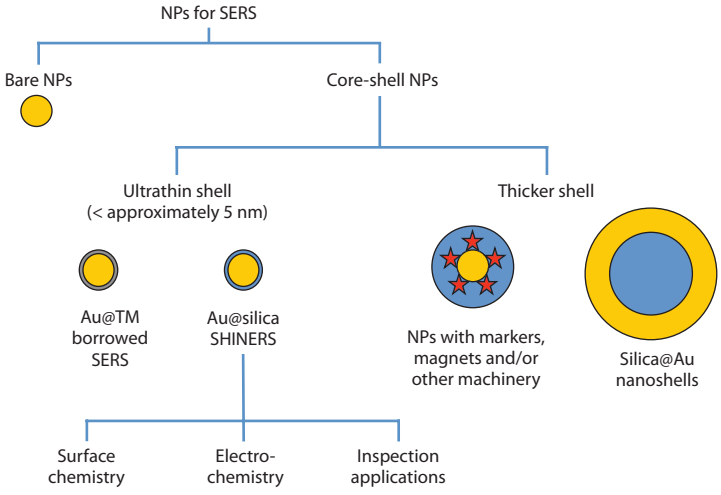


**Figure 1**

Core-shell nanoparticles (NPs) and shell-isolated nanoparticle-enhanced Raman spectroscopy (SHINERS). Abbreviations: SERS, surface-enhanced Raman scattering; TM, transition metal.

risk of interference. Then the weakly enhancing or nonenhancing materials that can be examined by SERS are not limited to those that can be coated onto a coinage metal NP in the form of an ultrathin shell. As we indicate in **Figure 1**, applications may be found in surface chemistry, electrochemistry, and inspection. We note that much interest has also been expressed in the use of coinage metal@coinage metal and coinage metal@polymer core-shell NPs for SERS (65–69).

## 1.3. The Advantages of Our Shell-Isolated Nanoparticle-Enhanced Raman Spectroscopy Method over Other Methods

To obtain a strong SERS signal with ease, a nanostructured substrate of Au, Ag, or Cu is required (Section 1.1). Various strategies have been developed to expand the SERS application to other materials. Some of these strategies include placing a nanostructured coinage metal in direct contact with the weakly enhancing or nonenhancing material by electrochemical deposition or thermal vapor deposition (**Figure 2*a*,*b***), adding a shell of the material to a coinage metal NP by some wet chemical method (**Figure 2*c***), and exciting SPs at a sharp coinage metal tip that is then brought very close to the material (**Figure 2*d***).

The electrochemical deposition and thermal vapor deposition techniques can be used to place randomly roughened coinage metal surfaces in contact with weakly enhancing or nonenhancing materials. In the former method, a rough coinage metal surface is created by oxidation-reduction cycling (ORC). Metal atoms are converted to ions during the oxidation half-cycle, and they enter the aqueous electrolyte solution. Metal atoms are then reformed from their ions during the reduction half-cycle, and they are deposited back onto the electrode surface. Once a rough coinage metal surface has been prepared, a thin film of some weakly enhancing or nonenhancing metal is added by electrochemical deposition. Alternatively, a coinage metal island film can be placed in contact with a weakly enhancing or nonenhancing material by thermal vapor deposition. During formation of the coinage metal film, adatom mobility competes with metal crystallization to yield islands having sizes and morphologies that are dependent on the precise conditions used.

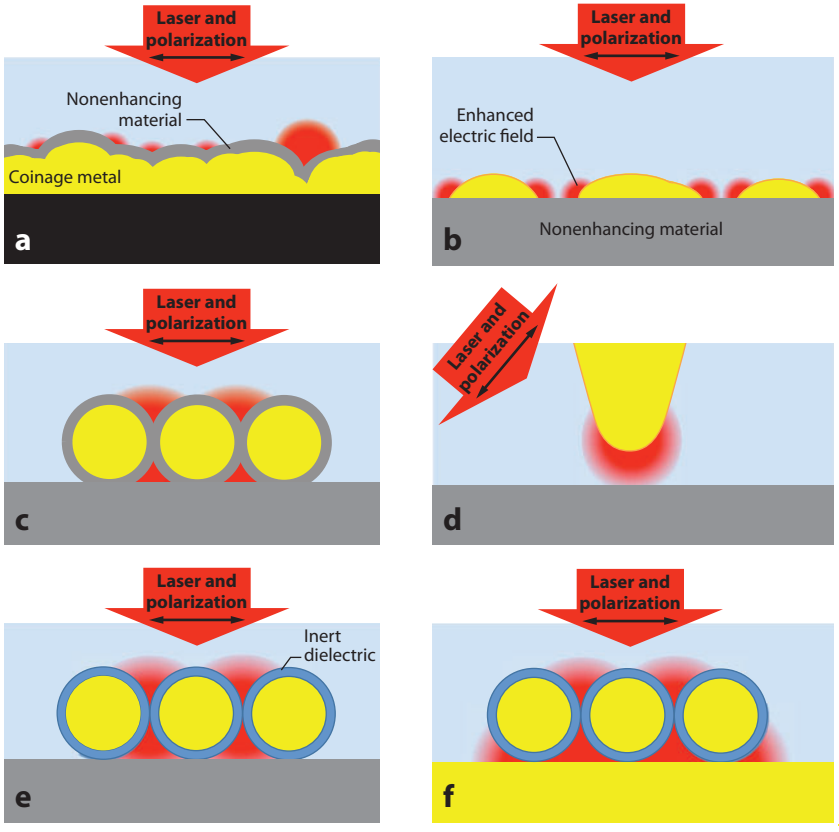


**Figure 2**

Different strategies for expanding the surface-enhanced Raman scattering application from coinage metals (*yellow*) to weakly enhancing or nonenhancing materials (*gray*). (*a*) Oxidation-reduction cycle roughening of a coinage metal is followed by electrochemical deposition of the material. (*b*) A coinage metal island film is deposited on top of the material. (*c*) An ultrathin shell of the material is added to a coinage metal nanoparticle (NP). (*d*) A sharp coinage metal tip is brought near the material. (*e*) An ultrathin shell of some inert dielectric (*blue*) is added to a coinage metal NP, and the NPs are then spread on top of the material. (*f*) The material in panel *e* is a single crystal of a coinage metal, and strongly enhanced electromagnetic fields emanate from the NP-to-substrate gaps in addition to the NP-to-NP gaps. Enhanced electric field strength is denoted by the red fog (theory-based depictions are provided in Section 2). Red arrows show the direction of incidence for the laser, and black arrows show the direction of polarization for the laser. Some of the incident laser light approaches at an angle in panels *a–c*, *e*, and *f* when a microscope objective with a large numerical aperture is employed.

ORC-roughened surfaces and island films were popular SERS substrates in the mid to late 1970s, 1980s, and 1990s, with some applications sought in analytical chemistry (70–73). These substrates are still used today (74, 75), but interest has shifted to other SERS substrates during the past ten years or so, especially to NPs. First, the maximum possible enhancement is much greater for NPs (28) than for surfaces such as island films (76). Second, enhancement from ORC-roughened surfaces and island films may be fairly reproducible when the laser spot is a few millimeters in diameter and an averaging effect is achieved, but that reproducibility decreases when a Raman microscope is employed and the laser spot is reduced to a few micrometers. NPs, in contrast, possess smaller-scale structural inconsistencies when they are used in solution or

tethered to a solid substrate in a uniformly packed monolayer, and sufficient averaging can occur in a micrometer-scale laser spot. Third, NP preparation does not require any special equipment. Lin et al. (77) provide further discussion of these two SERS substrates and further comparison with NPs.

**TERS:** tip-enhanced Raman spectroscopy

In some cases, an ultrathin shell of the weakly enhancing or nonenhancing material can be deposited onto a coinage metal NP (31, 78). This method has provided enough Raman signal enhancement for us to observe SERS from interfacial water on group VIIIB TMs (31, 79, 80). These TMs are SERS-active, but their activity is too weak, and the Raman scattering cross section of water too small, to allow this particular experiment to be done without assistance from an underlying coinage metal. Average EFs of up to five orders of magnitude may be obtained from coinage metal@TM NPs (31), but field strength is attenuated exponentially with increasing shell thickness, so the shell must be thin enough to permit the enhancement required for a given experiment. In contrast, the shell must be free from pinholes, and uniformity of the shell is easier to achieve as the shell becomes thicker. Furthermore, the shell must be thick enough to possess bulk properties if conclusions about the bulk are to be drawn. Thus, a delicate balance between SERS intensity versus shell uniformity and shell properties must be attained before high-quality, meaningful data can be acquired, and the time-consuming process of shell thickness optimization must be carried out for each new system studied (i.e., for each new shell material). A further problem commonly encountered when one is working with NPs is unwanted aggregation (e.g., during centrifuge-based cleaning).

Tip-enhanced Raman spectroscopy (TERS) combines scanning probe microscopy with Raman spectroscopy by placing a Au tip or a Ag tip close to the surface of interest and then illuminating the tip with light to generate LSPs at the apex (31, 81–86). Hence, field may be concentrated in the vicinity of a weakly enhancing or nonenhancing material, and SERS may be obtained from molecules located there. We have used this method to probe single crystals of Au and Pt (31, 87–90), which are atomically flat and therefore do not support the SP modes that are required for SERS when the tip is absent. When a TM is added to a coinage metal NP by some wet chemical technique, the TM shell is polycrystalline; thus, the ability to probe single crystals is a distinct advantage of TERS over the coinage metal@TM borrowed SERS strategy shown in **Figure 2*c***. Note that the spatial resolution offered by TERS (~10 nm at present) is important for the study of single molecules and molecular electronics devices, and is considered one of the greatest advantages of this technique. A number of drawbacks are associated with TERS, however. As is the case when ORC-roughened surfaces or island films are used to generate the enhancement, special equipment is required. In this case, the TERS setup is very expensive and quite sophisticated. Theoretically, the TERS EF may be as large as ten orders of magnitude (31), but the TERS signal is collected from a very small area of the sample so the absolute intensity of light detected is quite weak. When the tip-to-substrate distance becomes very small, probe/analyte molecules may jump from the sample (e.g., a single crystal of Au or Pt) to the tip (polycrystalline Au or Ag) and lead to undesirable peaks in the TERS spectrum. If the tip is submersed in solution for electrochemical or biological measurements, solution components may stick to the tip and again cause undesirable peaks in the TERS spectrum. Furthermore, problems associated with the air-water interface (such as additional scattering and distortion of the optical path) arise when the tip is submersed in solution, and such problems lead to a decrease in signal intensity. Schmid et al. (91) address the challenges encountered when performing TERS in situ.

All the shortcomings described above may be circumvented, at least to a large extent, by use of our SHINERS technique (**Figure 2*e*, *f***). In the following paragraphs, we describe progress with respect to sensitivity and reproducibility, spectral accuracy, and convenience.

We first discuss improvements to sensitivity and reproducibility. Enhancement from our SHINERS NPs is comparable to that obtained from ORC-roughened surfaces and island films, and coinage metal@TM NPs. With respect to TERS, each SHINERS NP can scatter light as a tip, so the equivalent of ~1,000 tips may be excited at the same time when SHINs having a 55-nm core fill a 2-μm laser spot. Because the absolute intensity of light detected is much greater for SHINERS than it is for TERS, additional scattering and distortion of the optical path at the air-water interface during in situ experiments do not matter as much. The price we pay for increasing sensitivity in this way, however, is a loss of the TERS spatial resolution. SHINERS NPs can be used in solution or tethered to a solid substrate in a uniformly packed monolayer (by attaching a trimethoxysilane-based linker to the glass shell), thereby increasing SERS-measurement reproducibility.

The second advantage of our SHINERS technique is improved spectral accuracy. When a TM shell is added to a coinage metal NP, the shell must be thick enough that electronic and morphological changes induced by contact with the coinage metal core, and associated with the nanoscale quantity of material present, become insignificant. If the shell is not sufficiently thick, inferences about the bulk must be made from the perturbed nanostructure—a dubious approach at best. When SHINERS NPs are spread over a TM surface, however, the unperturbed bulk material is probed (single crystals as well as polycrystalline samples can be investigated by SHINERS, and this advantage exists for both). In TERS, signal from the probe/analyte molecule on the tip can result in peaks that mislead spectral interpretation (because such peaks are irrelevant to the system of interest) and/or peaks that interfere with spectral interpretation (because such peaks overlap with peaks that arise from the system of interest). When our SHINERS method is employed, the probe/analyte molecule cannot come into direct contact with the enhancing surface, and this problem is alleviated. SHINERS NPs may also be spread over a surface to be submersed in aqueous solution for electrochemical or biological measurements without components of that environment adsorbing directly on the enhancing surface.

The third advantage of our SHINERS technique is convenience. Our SHINs can be prepared quickly and easily by wet chemical techniques, and no special equipment is required. When coinage metal@TM NPs are used, shell thickness must be optimized for each new system studied; but when SHINERS is employed, shell thickness need only be optimized for a few different shell materials before some SHIN will be compatible with any given system. Finally, the shell inhibits untimely NP aggregation.

## 2. ELECTRIC FIELD DISTRIBUTION AND ENHANCEMENT

The finite-difference time-domain (FDTD) method is a numerical one that can be used to determine how electromagnetic waves interact with objects, based on their material properties, by solving Maxwell's equations (92). To understand electric field distribution and enhancement about our SHINs, we modeled a 2 × 2 array of SHINERS NPs on a perfectly smooth Au surface and calculated the surrounding field strength by FDTD (**Figure 3**).

Regions of enhanced field strength exist in the SHIN-to-SHIN gaps as well as in the SHIN-to-substrate gaps. However, field distribution and enhancement in the plane formed by the latter are more important because of the way our SHINs are used. If the shell is pinhole free and the probe is not adsorbed on the shell, a substrate-probe-SHIN sandwich configuration is created with the probe located primarily in this plane. Therefore, nearly all of the Raman signal comes from the probe on the surface of interest.

The calculations show that a maximum electric field enhancement of 140 and 85 times may be achieved for 55-nm Au@2 nm of silica and 55-nm Au@4 nm of silica, respectively. The associated

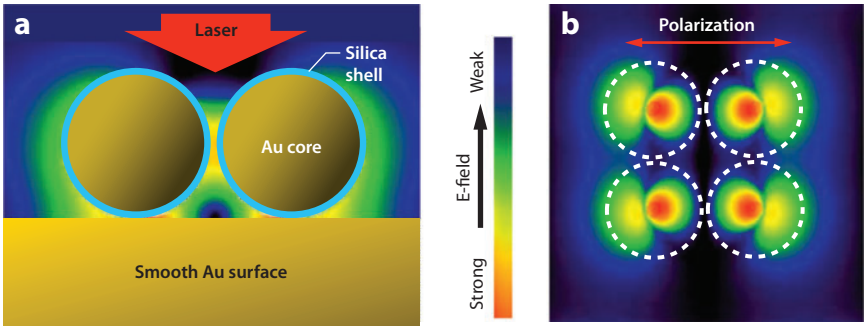


**Figure 3**

(*a*) Side view showing a 2 × 2 array of 55-nm Au@4-nm silica shell-isolated nanoparticles (SHINs) on a perfectly smooth Au surface. Finite-difference time-domain simulations were run with the incident light approaching vertically from the top. (*b*) Top view showing electric field (E-field) distribution contours in the plane between our SHINs and the smooth Au substrate, where probe molecules would lie during a typical SHIN-enhanced Raman spectroscopy experiment. Polarization of the 633-nm incident light is as indicated.

Raman scattering EFs are $4 \times 10^8$ and $5 \times 10^7$, respectively. The calculations also show that these maximum values depend on the interparticle distance, but not critically. If the 2 × 2 array is replaced by a single 55-nm Au@4 nm of silica SHIN, field enhancement drops from 85 to 55 times, and the Raman EF drops from $5 \times 10^7$ to $9 \times 10^6$. This is to say that the field enhancement and the Raman EF are still large in the single-particle case, and in practice, our SHINs do not need to be packed in a dense array to generate a strong signal.

The intensity of Raman scattering from a molecule located between two signal-enhancing particles decreases dramatically as the distance between them increases, plasmon coupling decreases, and a transition is made to the isolated-particle case (15, 16). The situation for a molecule between a particle and a surface is expected to be similar, and therefore SHINERS intensity from a probe located in the SHIN-to-substrate boundary plane should decrease rapidly with increasing shell thickness. To test for this, we spread 55-nm Au@2-nm silica, 55-nm Au@4-nm silica, 55-nm Au@6-nm silica, 55-nm Au@8-nm silica, 55-nm Au@10-nm silica, and 55-nm Au@20-nm silica SHINs over a smooth Au surface and used pyridine as the probe. The resulting spectra are presented in **Figure 4*a***, where it may be seen that, as expected, intensity decreases as the shell thickness increases. To show the nature of the relationship more clearly, we plot the area of the 1,013 $cm^{-1}$ peak against shell thickness in **Figure 4*b***. Integrated intensities were normalized by the 2-nm shell thickness integrated intensity, and error bars denote 20% of the result.

The field strength information that we obtained by FDTD may be correlated with these experimentally obtained Raman intensities because in a first approximation, SERS intensity scales with the fourth power of electric field strength (15, 16). Panels *c* and *d* of **Figure 4** allow field distribution and enhancement in the SHIN-to-substrate boundary plane for 2-nm and 8-nm silica shells to be compared visually. The maximum field intensity is greater for the 2-nm shell than the 8-nm shell. Because the distribution of field strength is not uniform, we integrated over the whole area. The resulting average field strength values were also normalized using the 2-nm shell thickness value and plotted in **Figure 4*b***. The trend in the experimental SHINERS intensity and the trend in the electric field strength at the SHIN-to-substrate boundary match well, indicating that SHINERS NPs operate according to our proposed mechanism.

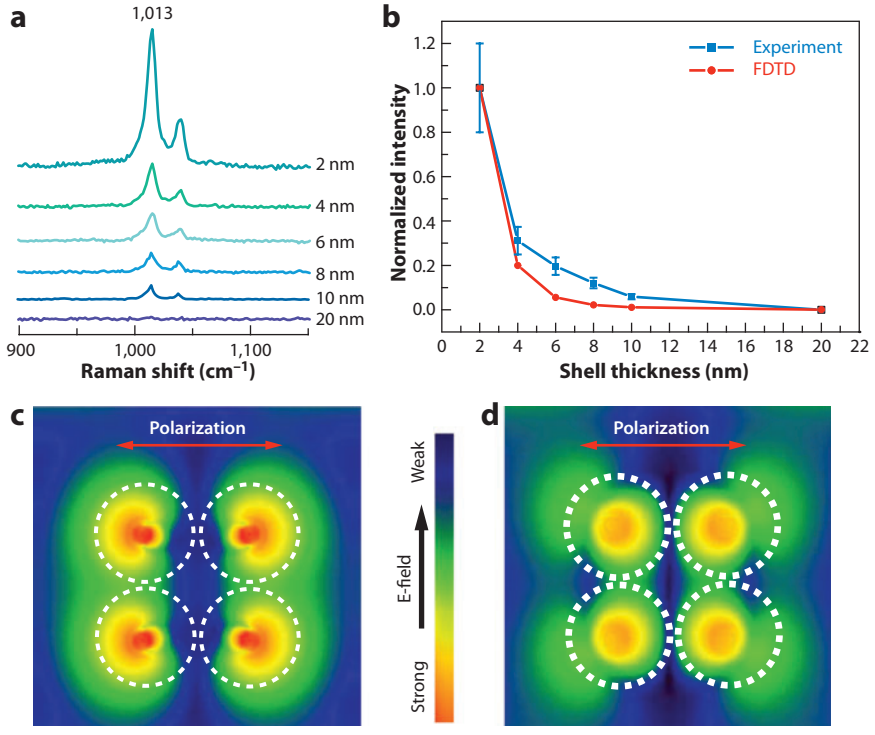


**Figure 4**

The dependence of shell-isolated nanoparticle-enhanced Raman spectroscopy (SHINERS) intensity on shell thickness. (*a*) SHINERS spectra were acquired for pyridine on a smooth Au surface. The silica shell thickness is given for each spectrum. (*b*) Experimental SHINERS intensities, normalized using data for the 2-nm shell, are plotted against shell thickness (*blue squares*). The error bars denote 20% of each value. Theoretical intensity results obtained by the finite-difference time-domain (FDTD) method, normalized using data for the 2-nm shell, are overlaid for comparison (*red circles*). (*c*,*d*) Top view of electric field (E-field) distribution, as calculated by FDTD, in the plane between our shell-isolated nanoparticles and a smooth Au surface. These images are similar to the image in **Figure 3*b*** except that these are for (*c*) 2-nm and (*d*) 8-nm silica instead of for 4-nm silica.

## 3. EXPERIMENTAL PROCEDURES

### 3.1. Synthesis and Purification of Our Shell-Isolated Nanoparticles

**Figure 5** provides a schematic overview of the procedure we use to create our SHINs. All the following reactions and cleaning procedures are carried out using 18.2 MΩ $cm^{-1}$ ultrapure water.

The Au core is prepared according to Frens's (93) method. First, 200 ml of 0.29-mM (0.010-wt%) chloroauric acid are brought to a boil in a round-bottom flask. Then, to obtain Au NPs with a 55-nm diameter, 1.4 ml of 39-mM (1.0-wt%) trisodium citrate are added quickly to the boiling solution. Smaller-sized NPs may be obtained by increasing the concentration of trisodium citrate, and larger-sized NPs may be obtained by decreasing this concentration. The mixture is refluxed with stirring for 40 min and is then allowed to cool to room temperature.

Au@silica SHINs are prepared by placing 30 ml of the Au NP solution into a round-bottom flask, adding 0.4 ml of 1-mM (3-aminopropyl)trimethoxysilane, and stirring for 15 min

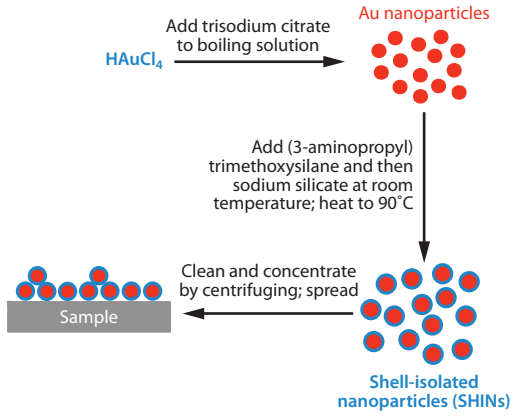


**Figure 5**

Schematic illustration of our shell-isolated nanoparticle (SHIN) synthesis.

at room temperature. A 27% solution of sodium silicate, purchased from Sigma-Aldrich® (**http://www.sigmaaldrich.com**), is diluted to 0.54% and adjusted to pH = 9.5–11.0 using hydrochloric acid. Subsequently, 3.2 ml of the diluted and acidified sodium silicate solution are added to the reaction mixture, and the mixture is stirred for 3 more min at room temperature. The solution is then heated to 90°C and stirred for a period of time that depends on the desired silica shell thickness: 20 min, 1 h, 2 h, 4 h, 8 h, or 20 h to coat the Au core with a thickness of approximately 2 nm, 4 nm, 6 nm, 8 nm, 10 nm, or 20 nm, respectively. This elevated temperature is an important modification to the coating procedure used by Liz-Marzán et al. (94) because otherwise, growing a shell 2–4 nm thick takes 24 h. The round-bottom flask is then cooled in an ice bath with stirring, which slows the reaction dramatically. Some of the resulting solution is placed into test tubes and centrifuged at 5,000 rpm for 15 min. The supernatant is removed, the concentrated SHINs at the bottom of each test tube are diluted, and the SHINs are centrifuged again. The supernatant is removed a second time and clean, concentrated SHINs are obtained from the bottoms of the test tubes.

## 3.2. Characterization of Our Shell-Isolated Nanoparticles

Two shell characteristics are important if our SHINs are to be used as an effective general tool for the acquisition of reliable SERS data: The shell must be ultrathin, and it should be pinhole free. In this section, we describe our procedures for testing shell thickness and continuity.

SHINs with different silica shell thicknesses may be prepared by altering the shell formation heating time (Section 3.1). To confirm the shell thickness, we use high-resolution transmission electron microscopy. Some typical images are provided in **Figure 6**.

To test the silica shell for a lack of pinholes, 10 μl of the clean, concentrated SHIN solution are placed on a silicon wafer and dried under vacuum. Next, 20 μl of 10-mM pyridine solution are added, and a quartz coverslip is placed on top. Pyridine is adsorbed on Au, but it is not strongly adsorbed on silica or silicon; thus, a SHINERS signal is obtained when pinholes are present in the shell but not when pinholes are absent. We recommend that the unknown sample be run with negative and positive controls for comparison. **Figure 7** shows the spectrum obtained from a perforated 1-nm shell, which may be used as a negative control, and the lack of signal from a well-formed 4-nm shell, which may be used as a positive control.

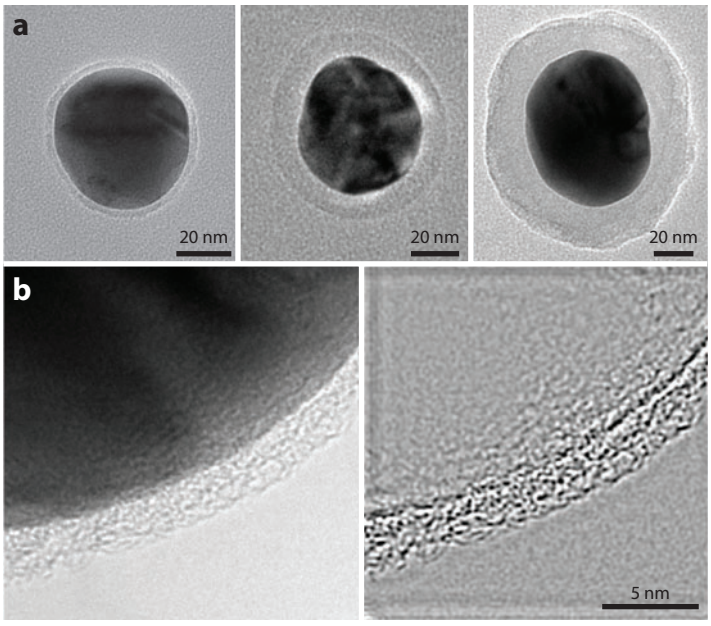


**Figure 6**

(*a*) High-resolution transmission electron microscopy (HR-TEM) images of Au@silica nanoparticles (NPs) with different silica shell thicknesses. (*b*) HR-TEM images of a Au@silica NP with a 2-nm shell.

## 4. SURFACE CHEMISTRY

### 4.1. Thiocyanate on Au(100) and Au(111)

Single-crystal surfaces cannot normally be examined by SERS because they are smooth and therefore do not support SP modes. Examination of smooth surfaces may be carried out, however, if NPs are spread on top and used to enhance the intensity of the incident (and Raman-scattered)

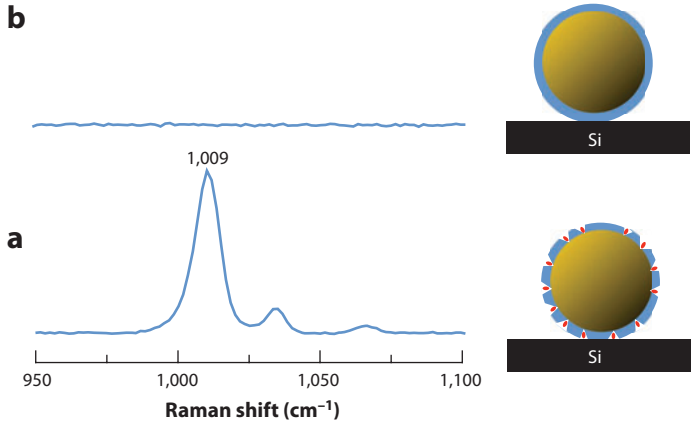


**Figure 7**

Surface-enhanced Raman scattering test for a lack of pinholes in the shell. These shell-isolated nanoparticle-enhanced Raman spectra were obtained using 55-nm Au@1-nm silica nanoparticles (NPs) (with pinholes, *a*) and 55-nm Au@4-nm silica NPs (without pinholes, *b*) on silicon wafers in 10-mM pyridine.

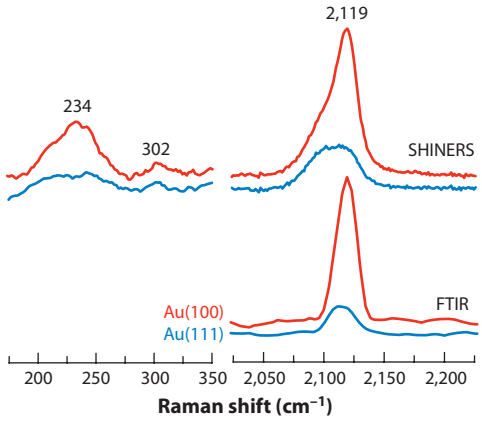


**Figure 8**

Comparison of shell-isolated nanoparticle-enhanced Raman spectroscopy (SHINERS) with Fourier transform infrared spectroscopy (FTIR) for thiocyanate ($SCN^-$) on Au(100) and Au(111). The counterelectrode was Pt, the potential was held at 0.0 V versus a saturated calomel electrode, and the solution employed was 0.1 M in $NaClO_4$ and 0.01 M in NaSCN. The excitation wavelength was 633 nm.

light. In this situation, it is important that the probe molecule be adsorbed on the single crystal but not on the NPs, which may be polycrystalline or even composed of a different metal. Otherwise, signal from the probe on the NPs may interfere with or mislead interpretation of the spectrum of the probe on the single crystal. Our SHINs, which have a protective glass coating, are therefore perfectly suited for the study of single crystals by SERS.

We have carried out such experiments using thiocyanate ($SCN^-$), which is not adsorbed on glass, to probe Au(100) and Au(111) electrode surfaces. SHINERS spectra obtained at 0.0 V relative to a saturated calomel electrode (SCE) are presented in the top portion of **Figure 8**. The signals obtained from $SCN^-$ on Au(100) and Au(111) are quite different. In the low–wave number region, peaks are seen for Au(100) at 234 and 302 $cm^{-1}$ with a height ratio of 5:1. These bands have been assigned to Au-S stretching of S-bound $SCN^-$ and to Au-N stretching of N-bound $SCN^-$, respectively (95–97). The height ratio of these two bands is reduced to 2.5:1 in the spectrum of $SCN^-$ on Au(111), indicating that a greater fraction of $SCN^-$ is bound to Au by the N atom. Spectral features in the high–wave number region confirm this interpretation. Here, a strong sharp peak is seen for Au(100) at 2,119 $cm^{-1}$. This peak has been assigned to the C-N stretching mode of S-bound $SCN^-$ (95–97). For Au(111), the peak is weaker and broader. Figure 1 in Reference 95 and figure 4 in Reference 96 show that the peak becomes weaker and broader as the orientation of $SCN^-$ changes, with the N-bound fraction increasing and the S-bound fraction decreasing.

We obtained similar results in the high–wave number region by unenhanced Fourier transform infrared (FTIR) spectroscopy: A strong sharp peak was observed at 2,119 $cm^{-1}$ for Au(100), and it appeared weaker and broader for Au(111). These data are presented in the bottom portion of **Figure 8**. The low–wave number region is inaccessible by IR spectroscopy under electrochemical conditions, and the information that SHINERS can provide about the bonding of molecules to single crystals via this spectral region is one of the advantages of our technique. Another advantage lies in the fact that when IR and Raman data are acquired for the same spectral region, the information is in general complementary rather than identical (1–3), so the acquisition of both kinds of data is beneficial for a full understanding of surface structures and processes.

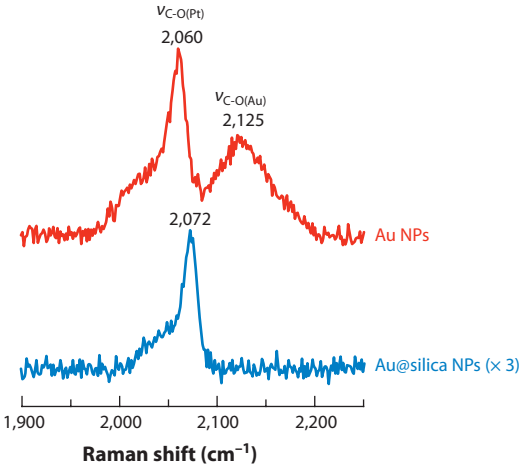


**Figure 9**

Surface-enhanced Raman scattering spectra of carbon monoxide (CO) on Pt(111) obtained using bare Au nanoparticles (NPs) (*top*) and our shell-isolated nanoparticles (*bottom*) as the Raman signal–enhancing substrate. The counterelectrode was Pt, the potential was held at 0.0 V versus a saturated calomel electrode, and the solution employed was 0.1 M in $HClO_4$ and saturated with CO gas. The excitation wavelength was 633 nm.

## 4.2. Carbon Monoxide on Pt(111)

The method described in Section 4.1 may be extended to metal surfaces other than Au, as well as to semiconductor surfaces. Then if bare Au NPs are spread on top of the single crystal and used to obtain SERS from a probe, at least two different problems can result. First, adsorption of the probe on the Au may lead to additional peaks. Second, electrical contact between the bare Au NPs and the single crystal may lead to a charge transfer that can perturb the electronic structure of the surface under study and cause shifting of the probe's vibrational bands (98).

These problems are illustrated by carbon monoxide (CO) on Pt(111) in **Figure 9**. When bare Au NPs are spread over Pt(111) and the SERS spectrum of adsorbed CO is acquired at 0.0 V versus SCE, two peaks are observed: one at 2,060 cm$^{-1}$ that is due to C-O(Pt) stretching (99) and one at 2,125 cm$^{-1}$ that is due to C-O(Au) stretching (99). The band at 2,125 cm$^{-1}$ is undesirable because it is irrelevant to CO adsorption on a Pt surface. Moreover, this band overlaps with the C-O(Pt) peak and thus complicates the procedure required for its integration. Electrical contact between these two metals results in charge transfer from Au to Pt, both in the bulk [the work functions for polycrystalline Au and Pt(111) are 5.1 and 5.7 eV, respectively (100)] and at the nanoscale (101). Because the Pt surface has more negative charge, we see a shift in the position of the C-O(Pt) band from 2,072 cm$^{-1}$ to 2,060 cm$^{-1}$ (**Figure 9**). In SHINERS, chemical and electrical isolation of the Au core is achieved via the silica shell. Hence, both of these problems are resolved and the true spectrum of CO on Pt(111) can be obtained (**Figure 9**).

**Hydrogen evolution:** when sufficiently negative potentials are reached during an electrochemical experiment, aqueous solvent is converted to hydrogen gas at the surface of the working electrode:
$2H_2O + 2e^- \rightarrow H_2 + 2OH^-$

## 5. ELECTROCHEMISTRY: HYDROGEN ON Rh(111)

Hydrogen evolution is a common problem in electrochemical systems when the applied potential is sufficiently negative for the reductive dissociation of water to occur (102). We have used both the borrowed SERS approach (**Figure 2*c***) and SHINERS (**Figure 2*e***) to examine hydrogen

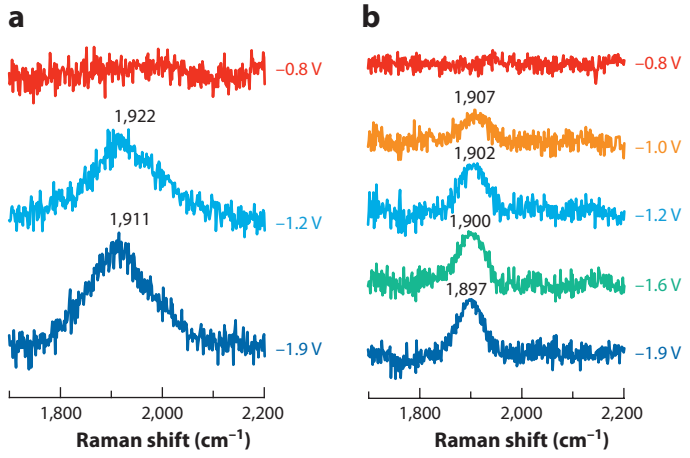


**Figure 10**

(*a*) Surface-enhanced Raman scattering spectra of hydrogen on Au@Rh/smooth Rh and (*b*) shell-isolated nanoparticle-enhanced Raman spectra of hydrogen on Rh(111). The solution employed was 0.1 M in $NaClO_4$, a Pt wire served as the counterelectrode, and the potentials given are relative to a saturated calomel electrode. The excitation wavelength was 633 nm.

adsorption on Rh. In the former of these two methods, 55-nm Au NPs were coated chemically with 1–2 nm of Rh, and then the Au@Rh NPs were spread over a smooth Rh electrode. Rh is polycrystalline when it is deposited on a Au NP by wet chemical techniques, and a polycrystalline electrode was also used. In the SHINERS approach, 55-nm Au@1–2-nm silica SHINs were spread over a Rh(111) electrode. The Raman scattering cross section of hydrogen is extremely small, and to obtain a stronger signal, it may be desirable to use a 1-nm silica shell with pinholes instead of a 2-nm silica shell without pinholes. Pinholes do not present a problem for the present system because hydrogen is not strongly adsorbed on Au, and a shell with some very small holes can still prevent electrical contact between the SHIN Au core and the Rh(111) surface.

The resulting spectra are shown in **Figure 10**. The potential was stepped in the negative direction, and hydrogen evolution began to take place at approximately −1.0 V. A shift in the position of the Rh-H stretching peak with applied potential (an electrochemical Stark effect) occurred for both systems. Furthermore, this peak is much narrower for the single crystal than for polycrystalline Rh. Each facet of a polycrystalline sample of an element may yield a slightly different position for a given adsorbate vibrational band, and if these facet-induced differences are not resolved, a single broad peak is observed. If one facet dominates the sample, however, the simplified spectrum appears as a narrower peak. This relationship between crystal structure and bandwidth has previously been discussed by our group (103).

A single crystal is a type of model system, and single crystals are used quite frequently in surface science. The results presented here (as well as those presented in Section 4) demonstrate that our SHINERS method can allow for the detection of thin probe/analyte films on these atomically flat surfaces by Raman spectroscopy, even under electrochemical conditions.

## 6. INSPECTION

SHINERS NPs may be applied to virtually any surface for the quick and easy identification of analytes. Potential applications lie in drug and explosives screening, environmental protection,

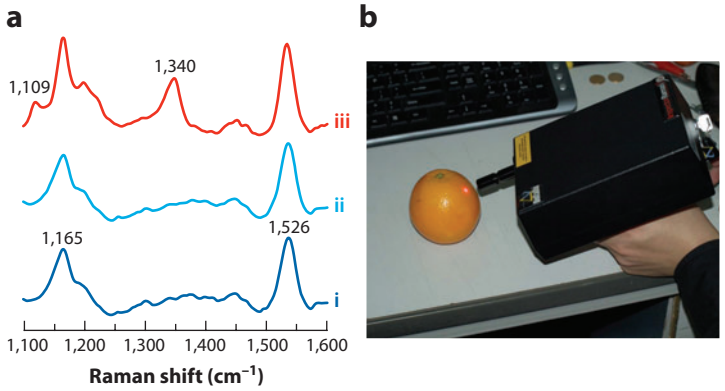


**Figure 11**

(*a*) The ordinary Raman spectra of clean and contaminated orange skins are given by curves *i* and *ii*, respectively. The shell-isolated nanoparticle-enhanced Raman spectrum of a contaminated orange skin is given by curve *iii*. The excitation wavelength was 785 nm, the laser power on the sample was 30 mW, and the acquisition time was 30 s. (*b*) A photograph of the experiment, which was conducted using a DeltaNu Inspector Raman$^{TM}$ spectrometer.

and food safety inspection. In order to demonstrate this we used a portable Raman spectrometer, and our SHINs, to detect a pesticide residue on an orange skin.

Our portable Raman spectrometer offers a 785-nm excitation source, but this wavelength does not match the ~600-nm SP resonance wavelength of our standard 55-nm spherical Au@silica SHINs (38). So to shift the SP resonance toward the laser wavelength, 20-nm by 60-nm Au nanorods were prepared according to Nikoobakht and El-Sayed (104) and used as the core. The resulting SHINs displayed an SP resonance at ~770 nm.

**Figure 11*a*** shows the ordinary Raman spectrum obtained from an orange peel before exposure to parathion pesticide. The bands at 1,165 and 1,526 $cm^{-1}$ are due to carotenoids (105) that occur naturally in citrus fruit. A solution of parathion in ethanol (0.1–1 mM) was then sprayed onto the orange peel and allowed to dry. The ordinary Raman spectrum was again collected, and this spectrum is shown in **Figure 11*a***. Due to the low sensitivity of normal Raman spectroscopy, the parathion residue was not detected. SHIN rods were then applied, and the SHINERS spectrum was recorded. Parathion bands may be seen at 1,109 and 1,340 $cm^{-1}$ (106) in **Figure 11*a***.

## 7. CONCLUDING DISCUSSION AND OUTLOOK

### 7.1. Concluding Discussion

In **Table 1** we group currently available Raman signal–enhancing structures into three broad categories: random nanostructures, ordered nanostructures, and complex nanostructures that are composed of more than one type of material. For each category, including three subdivisions of the last category, morphological generality, materials generality, and probe/analyte generality are rated on a five-point scale as poor, fair, good, very good, or excellent.

Work on SERS began in the mid 1970s, and during the next 25 years or so, ORC-roughened surfaces, island films, and surfaces covered with disordered NP aggregates dominated the literature. All these substrates possessed random features over which limited control could be exercised, so morphological generality is described as poor. Because they were composed of Au, Ag, or Cu, materials generality is also given as poor. The EFs obtained were high enough that a wide variety

**Table 1 Enhancement strategies and their generality**

| | Time frame | Example(s) | Morphological generality | Materials generality | Probe/analyte generality |
|---|---|---|---|---|---|
| Random nanostructures | Mid 1970s to 2000s | ORC-generated, island films, NP aggregates | Poor | Poor | Very good |
| Ordered nanostructures | 1990s to present | Tethered NPs, EBL-fabricated, FIB-milled | Good | Fair | Excellent |
| More complex (multicomponent) nanostructures | Mid 1990s to present | Core-shell NPs, coated nanostructures | Good | Good | Very good |
| | 2000s to present | TERS | Excellent | Excellent | Good |
| | Present | SHINERS | Excellent | Excellent | Very good |

Morphological generality, materials generality, and probe/analyte generality are rated on a five-point scale as poor, fair, good, very good, or excellent. Abbreviations: ORC, oxidation-reduction cycling; NP, nanoparticle; EBL, electron beam lithography; FIB, focused ion beam; TERS, tip-enhanced Raman spectroscopy; SHINERS, shell-isolated nanoparticle-enhanced Raman spectroscopy.



of probe/analyte molecules could be detected easily, and we call probe/analyte generality very good.

Ordered nanostructures revitalized SERS research and may be considered the second generation of SERS substrates. Examples include NPs tethered to a solid surface in a uniformly packed monolayer, substrates fabricated by electron beam lithography, and substrates prepared by focused ion beam milling. Here, control over the substrate's morphology at the nanoscale may be considered very good; but at the atomic level the morphology is only good as the surfaces are not structurally well-defined [except for some nanocubes with the (111) facet]. This control has led to greater EFs and to greater reproducibility. Greater EFs mean that weakly enhancing materials such as the group VIIIB TMs can be used with more success. In practice, however, most of these second-generation substrates are still composed of Au, Ag, or Cu, and materials generality is only slightly improved over that of the first-generation substrates. Greater EFs also mean improved probe/analyte generality when coinage metals are employed—molecules with lower Raman scattering cross sections can be, and are being, used in connection with these substrates.

The more complex nanostructures category is further divided into three subcategories. These include core-shell NPs and coated (ordered) nanostructures, TERS, and SHINERS.

As explained above in Sections 1.2 and 1.3, some weakly enhancing or nonenhancing material may be coated onto a coinage metal nanostructure as an ultrathin shell to obtain strong SERS from a molecule on the surface, thus improving materials generality. Most procedures deposit coatings that follow the morphology of the underlying ordered nanostructure in a fairly uniform way, so morphological generality is described as good here, as it was for the uncoated ordered nanostructure. Field strength at the coating's surface is weaker than field strength at the surface of the underlying coinage metal, so EFs are lower here than they were for the uncoated ordered nanostructure and probe/analyte generality is reduced from excellent for the uncoated ordered nanostructure to very good.

The TERS method was a conceptual breakthrough in that the signal amplifier was separated from the probed surface for the first time, and TERS may be used to examine a surface of any

morphology and any material. The EF may be large, but the signal originates from a very small region of the sample so the absolute intensity of light detected is still weak. Therefore, only probe/analyte molecules with large Raman scattering cross sections are appropriate for use with TERS.

Our SHINERS technique is in one sense an extension of the core-shell and coatings strategy already described. The reason for the shell and the way in which the NPs are used differ significantly in SHINERS, however, and a considerable step forward in generality is the result. The material of interest is no longer added to the SERS-active coinage metal; rather, an isolating shell is added and the structure is then spread onto a surface of any morphology and any material. So in another sense, SHINERS is an extension of what was accomplished for the first time with TERS: The signal amplifier is again separated from the probed surface. With the advent of SHINERS, SERS may be obtained from surfaces with the unlikely morphology of an atomically flat single crystal (Sections 4 and 5) and the unlikely material of an orange skin (Section 6). The EFs achieved with SHINERS are comparable to those achieved with core-shell NPs and coated (ordered) nanostructures, so the probe/analyte molecule generality is also comparable.



### 7.2. Outlook

With the advent of SHINERS, we expect a growing emphasis on the direct detection and identification of analytes by SERS. Here, SHINERS could be used to examine the surface of the skin, cells and tissues after biopsy, or surface chemistry as part of an industrial quality-control procedure. In addition to the direct detection and identification of analytes, we anticipate the in-depth characterization of probe-surface interactions for a wide variety of weakly enhancing and nonenhancing surfaces through detailed examination of their SHINERS spectra. Examples could include the probing of surface processes associated with catalysis and corrosion.

We also expect new structures to emerge. The SHIN surface could be modified with a trimethoxysilane-based linker, and then a biological receptor could be added or the SHINs could be attached to a solid substrate in a uniformly packed monolayer. Any incompatibilities that may exist between certain chemical systems and the currently available shells, which include silica and alumina (38), will vanish as we learn how new materials can be deposited to form a shell that is ultrathin and ideally pinhole free. Meanwhile, the shell-isolating concept may be applied to nanostructures other than NPs. As explained above in Section 1.1, this idea could be used to reduce the mobility of coinage metal atoms and therefore inhibit SERS-substrate deterioration. Finally, our SHINs could be used for other surface-enhanced spectroscopies such as fluorescence, infrared absorption, and nonlinear optical spectroscopies.

## DISCLOSURE STATEMENT

The authors are not aware of any affiliations, memberships, funding, or financial holdings that might be perceived as affecting the objectivity of this review.

## ACKNOWLEDGMENTS

We thank Z.L. Wang and R.N. Zare for helpful discussions. This work was supported by the National Science Foundation of China (21033007 and 20620130427) and by the Ministry of Science and Technology of China (2009CB930703, 2007DFC40440 and 2007CB935603).

## LITERATURE CITED


1. Smith E, Dent G. 2005. *Modern Raman Spectroscopy: A Practical Approach*. Chichester, UK: Wiley
2. Long DA. 2002. *The Raman Effect: A Unified Treatment of the Theory of Raman Scattering by Molecules*. Chichester, UK: Wiley
3. McCreery RL. 2000. *Chemical Analysis*, Vol. 157*: Raman Spectroscopy for Chemical Analysis*. New York: Wiley
4. Aroca R. 2006. *Surface-Enhanced Vibrational Spectroscopy*. Chichester, UK: Wiley
5. Le Ru EC, Etchegoin PG. 2009. *Principles of Surface-Enhanced Raman Spectroscopy and Related Plasmonic Effects*. Amsterdam/Oxford: Elsevier
6. Kneipp K, Moskovits M, Kneipp H, eds. 2006. *Topics in Applied Physics*, Vol. 103*: Surface-Enhanced Raman Scattering Physics and Applications*. Berlin/Heidelberg: Springer
7. Schlücker S, ed. 2011. *Surface Enhanced Raman Spectroscopy: Analytical, Biophysical and Life Science Applications*. Weinheim, Ger.: Wiley
8. Chang RK, Furtak TE, eds. 1982. *Surface Enhanced Raman Scattering*. New York: Plenum
9. Fleischmann M, Hill IR. 1984. Raman spectroscopy. In *Comprehensive Treatise of Electrochemistry*, Vol. 8*: Experimental Methods in Electrochemistry*, ed. RE White, JOM Bockris, BE Conway, E Yeager, pp. 373–432. New York: Plenum
10. Etchegoin PG, ed. 2009. New frontiers in surface-enhanced Raman scattering. *Phys. Chem. Chem. Phys.* (*Spec. Iss.*) 34:7333–512
11. Graham D, Goodacre R, eds. 2008. Surface enhanced Raman spectroscopy. *Chem. Soc. Rev.* (*Spec. Iss.*) 37:873–1076
12. Brown RJC, Cohen LF, Milton MJT, eds. 2006. Surface enhanced Raman spectroscopy. *Faraday Discuss.* (*Spec. Iss.*) 132:1–340
13. Tian Z-Q, ed. 2005. Surface enhanced Raman spectroscopy. *J. Raman Spectrosc.* (*Spec. Iss.*) 36:465–747
14. Stiles PL, Dieringer JA, Shah NC, Van Duyne RP. 2008. Surface-enhanced Raman spectroscopy. *Annu. Rev. Anal. Chem.* 1:601–26
15. Moskovits M. 1985. Surface-enhanced spectroscopy. *Rev. Mod. Phys.* 57:783–826
16. Moskovits M. 2005. Surface-enhanced Raman spectroscopy: a brief retrospective. *J. Raman Spectrosc.* 36:485–96
17. Pieczonka NPW, Aroca RF. 2005. Inherent complexities of trace detection by surface-enhanced Raman scattering. *ChemPhysChem* 6:2473–84
18. Bell SEJ, Sirimuthu NMS. 2008. Quantitative surface-enhanced Raman spectroscopy. *Chem. Soc. Rev.* 37:1012–24
19. Porter MD, Lipert RJ, Siperko LM, Wang G, Narayanan R. 2008. SERS as a bioassay platform: fundamentals, design, and applications. *Chem. Soc. Rev.* 37:1001–11
20. Smith WE. 2008. Practical understanding and use of surface enhanced Raman scattering/surface enhanced resonance Raman scattering in chemical and biological analysis. *Chem. Soc. Rev.* 37:955–64
21. Graham D, Faulds K. 2008. Quantitative SERRS for DNA sequence analysis. *Chem. Soc. Rev.* 37:1042–51
22. Banholzer MJ, Millstone JE, Qin L, Mirkin CA. 2008. Rationally designed nanostructures for surface-enhanced Raman spectroscopy. *Chem. Soc. Rev.* 37:885–97
23. Anker JN, Hall WP, Lyandres O, Shah NC, Zhao J, Van Duyne RP. 2008. Biosensing with plasmonic nanosensors. *Nat. Mater.* 7:442–53
24. Wang H, Brandl DW, Nordlander P, Halas NJ. 2007. Plasmonic nanostructures: artificial molecules. *Acc. Chem. Res.* 40:53–62
25. Willets KA, Van Duyne RP. 2007. Localized surface plasmon resonance spectroscopy and sensing. *Annu. Rev. Phys. Chem.* 58:267–97
26. Zayats AV, Smolyaninov II, Maradudin AA. 2005. Nano-optics of surface plasmon polaritons. *Phys. Rep.* 408:131–314
27. Barnes WL, Dereux A, Ebbesen TW. 2003. Surface plasmon subwavelength optics. *Nature* 424:824–30
28. Le Ru EC, Blackie E, Meyer M, Etchegoin PG. 2007. Surface enhanced Raman scattering enhancement factors: a comprehensive study. *J. Phys. Chem. C* 111:13794–803

29. Tian Z-Q, Ren B, Wu D-Y. 2002. Surface-enhanced Raman scattering: from noble to transition metals and from rough surfaces to ordered nanostructures. *J. Phys. Chem. B* 106:9463–83
30. Ren B, Liu G-K, Lian X-B, Yang Z-L, Tian Z-Q. 2007. Raman spectroscopy on transition metals. *Anal. Bioanal. Chem.* 388:29–45
31. Tian Z-Q, Ren B, Li J-F, Yang Z-L. 2007. Expanding generality of surface-enhanced Raman spectroscopy with borrowing SERS activity strategy. *Chem. Commun.* 2007:3514–34
32. Nie S, Emory SR. 1997. Probing single molecules and single nanoparticles by surface-enhanced Raman scattering. *Science* 275:1102–6
33. Kneipp K, Wang Y, Kneipp H, Perelman LT, Itzkan I, et al. 1997. Single molecule detection using surface-enhanced Raman scattering (SERS). *Phys. Rev. Lett.* 78:1667–70
34. Michaels AM, Nirmal M, Brus LE. 1999. Surface enhanced Raman spectroscopy of individual rhodamine 6G molecules on large Ag nanocrystals. *J. Am. Chem. Soc.* 121:9932–39
35. Xu H, Bjerneld EJ, Käll M, Borjesson L. 1999. Spectroscopy of single hemoglobin molecules by surface enhanced Raman scattering. *Phys. Rev. Lett.* 83:4357–60
36. Xu H, Aizpurua J, Käll M, Apell P. 2000. Electromagnetic contributions to single-molecule sensitivity in surface-enhanced Raman scattering. *Phys. Rev. E* 62:4318–24
37. Dieringer JA, Wustholz KL, Masiello DJ, Camden JP, Kleinman SL, et al. 2009. Surface-enhanced Raman excitation spectroscopy of a single rhodamine 6G molecule. *J. Am. Chem. Soc.* 131:849–54
38. Li J-F, Huang Y-F, Ding Y, Yang Z-L, Li S-B, et al. 2010. Shell-isolated nanoparticle–enhanced Raman spectroscopy. *Nature* 464:392–95
39. Withnall R, Chowdhry BZ, eds. 2008. *Proceedings of the XXIst International Conference on Raman Spectroscopy*. London: IM Publ.
40. Kneipp K, Kneipp H, Itzkan I, Dasari RR, Feld MS. 1999. Ultrasensitive chemical analysis by Raman spectroscopy. *Chem. Rev.* 99:2957–75
41. Laserna JJ. 1993. Combining fingerprinting capability with trace analytical detection: surface-enhanced Raman spectrometry. *Anal. Chim. Acta* 283:607–22
42. Kambe K. 1955. Cohesive energy of noble metals. *Phys. Rev.* 99:419–22
43. Park H, Lee S, Chen L, Lee EK, Shin SY, et al. 2009. SERS imaging of HER2-overexpressed MCF7 cells using antibody-conjugated gold nanorods. *Phys. Chem. Chem. Phys.* 11:7444–49
44. Narayanan R, Lipert RJ, Porter MD. 2008. Cetyltrimethylammonium bromide–modified spherical and cube-like gold nanoparticles as extrinsic Raman labels in surface-enhanced Raman spectroscopy based heterogeneous immunoassays. *Anal. Chem.* 80:2265–71
45. Doering WE, Nie S. 2003. Spectroscopic tags using dye-embedded nanoparticles and surface-enhanced Raman scattering. *Anal. Chem.* 75:6171–76
46. Mulvaney SP, Musick MD, Keating CD, Natan MJ. 2003. Glass-coated, analyte-tagged nanoparticles: a new tagging system based on detection with surface-enhanced Raman scattering. *Langmuir* 19:4784–90
47. Gong J-L, Jiang J-H, Liang Y, Shen G-L, Yu R-Q. 2006. Synthesis and characterization of surface-enhanced Raman scattering tags with $Ag/SiO_2$ core-shell nanostructures using reverse micelle technology. *J. Colloid Interface Sci.* 298:752–56
48. Gong J-L, Jiang J-H, Yang H-F, Shen G-L, Yu R-Q, Ozaki Y. 2006. Novel dye-embedded core-shell nanoparticles as surface-enhanced Raman scattering tags for immunoassay. *Anal. Chim. Acta* 564:151–57
49. Kim J-H, Kim J-S, Choi H, Lee S-M, Jun B-H, et al. 2006. Nanoparticle probes with surface enhanced Raman spectroscopic tags for cellular cancer targeting. *Anal. Chem.* 78:6967–73
50. Gong J-L, Liang Y, Huang Y, Chen J-W, Jiang J-H, et al. 2007. $Ag/SiO_2$ core-shell nanoparticle-based surface-enhanced Raman probes for immunoassay of cancer marker using silica-coated magnetic nanoparticles as separation tools. *Biosens. Bioelectron.* 22:1501–7
51. Liang Y, Gong J-L, Huang Y, Zheng Y, Jiang J-H, et al. 2007. Biocompatible core-shell nanoparticle-based surface-enhanced Raman scattering probes for detection of DNA related to HIV gene using silica-coated magnetic nanoparticles as separation tools. *Talanta* 72:443–49
52. Xia L, Kim NH, Kim K. 2007. Stabilization of hydroxyl-group-terminated SERS-marker molecules on μAg particles by silanization. *J. Colloid Interface Sci.* 306:50–55
53. Brown LO, Doorn SK. 2008. A controlled and reproducible pathway to dye-tagged, encapsulated silver nanoparticles as substrates for SERS multiplexing. *Langmuir* 24:2277–80

54. Sha M-Y, Xu H, Natan MJ, Cromer R. 2008. Surface-enhanced Raman scattering tags for rapid and homogeneous detection of circulating tumor cells in the presence of human whole blood. *J. Am. Chem. Soc.* 130:17214–15
55. Jun B-H, Noh MS, Kim G, Kang H, Kim J-H, et al. 2009. Protein separation and identification using magnetic beads encoded with surface-enhanced Raman spectroscopy. *Anal. Biochem.* 391:24–30
56. Küstner B, Gellner M, Schütz M, Schöppler F, Marx A, et al. 2009. SERS labels for red laser excitation: silica-encapsulated SAMs on tunable gold/silver nanoshells. *Angew. Chem. Int. Ed.* 48:1950–53
57. Jun B-H, Noh MS, Kim J, Kim G, Kang H, et al. 2010. Multifunctional silver-embedded magnetic nanoparticles as SERS nanoprobes and their applications. *Small* 6:119–25
58. Liu S, Han M-Y. 2010. Silica-coated metal nanoparticles. *Chem. Asian J.* 5:36–45
59. Oldenburg SJ, Westcott SL, Averitt RD, Halas NJ. 1999. Surface enhanced Raman scattering in the near infrared using metal nanoshell substrates. *J. Chem. Phys.* 111:4729–35
60. Jackson JB, Westcott SL, Hirsch LR, West JL, Halas NJ. 2003. Controlling the surface enhanced Raman effect via the nanoshell geometry. *Appl. Phys. Lett.* 82:257–59
61. Jackson JB, Halas NJ. 2004. Surface-enhanced Raman scattering on tunable plasmonic nanoparticle substrates. *Proc. Natl. Acad. Sci. USA* 101:17930–35
62. Lal S, Grady NK, Kundu J, Levin CS, Lassiter JB, Halas NJ. 2008. Tailoring plasmonic substrates for surface enhanced spectroscopies. *Chem. Soc. Rev.* 37:898–911
63. McNay G, Docherty FT, Graham D, Smith WE, Jordan P, et al. 2004. Visual observations of SERRS from single silver-coated silica microparticles within optical tweezers. *Angew. Chem. Int. Ed.* 43:2512–14
64. Bálint Š, Kreuzer MP, Rao S, Badenes G, Miškovský P, Petrov D. 2009. Simple route for preparing optically trappable probes for surface-enhanced Raman scattering. *J. Phys. Chem. C* 113:17724–29
65. Cao YC, Jin R, Mirkin CA. 2002. Nanoparticles with Raman spectroscopic fingerprints for DNA and RNA detection. *Science* 297:1536–40
66. Cui Y, Ren B, Yao J-L, Gu R-A, Tian Z-Q. 2006. Synthesis of $Ag_{core}Au_{shell}$ bimetallic nanoparticles for immunoassay based on surface-enhanced Raman spectroscopy. *J. Phys. Chem. B* 110:4002–6
67. Qian X, Peng X-H, Ansari DO, Yin-Goen Q, Chen G-Z, et al. 2008. In vivo tumor targeting and spectroscopic detection with surface-enhanced Raman nanoparticle tags. *Nat. Biotechnol.* 26:83–90
68. Yang M, Chen T, Lau WS, Wang Y, Tang Q, et al. 2009. Development of polymer-encapsulated metal nanoparticles as surface-enhanced Raman scattering probes. *Small* 5:198–202
69. Lim D-K, Jeon K-S, Kim HM, Nam J-M, Suh YD. 2010. Nanogap-engineerable Raman-active nanodumbbells for single-molecule detection. *Nat. Mater.* 9:60–67
70. Carrabba MM, Edmonds RB, Rauh RD. 1987. Feasibility studies for the detection of organic surface and subsurface water contaminants by surface-enhanced Raman spectroscopy on silver electrodes. *Anal. Chem.* 59:2559–63
71. Mosier-Boss PA, Lieberman SH. 1999. Feasibility studies for the detection of volatile organic compounds in the gas phase using microelectrode sensors. *J. Electroanal. Chem.* 460:105–18
72. Sockalingum GD, Beljebbar A, Morjani H, Angiboust JF, Manfait M. 1998. Characterization of island films as surface-enhanced Raman spectroscopy substrates for detecting low antitumor drug concentrations at single cell level. *Biospectroscopy* 4:S71–78
73. Stokes DL, Pal A, Narayanan VA, Vo-Dinh T. 1999. Evaluation of a chemical vapor dosimeter using polymer-coated SERS substrates. *Anal. Chim. Acta* 399:265–74
74. Wang A, Huang Y-F, Sur UK, Wu D-Y, Ren B, et al. 2010. In situ identification of intermediates of benzyl chloride reduction at a silver electrode by SERS coupled with DFT calculations. *J. Am. Chem. Soc.* 132:9534–36
75. Anema JR, Brolo AG, Felten A, Bittencourt C. 2010. Surface-enhanced Raman scattering from polystyrene on gold clusters. *J. Raman Spectrosc.* 41:745–51
76. Otto A. 2006. On the significance of Shalaev's "hot spots" in ensemble and single-molecule SERS by adsorbates on metallic films at the percolation threshold. *J. Raman Spectrosc.* 37:937–47
77. Lin X-M, Cui Y, Xu Y-H, Ren B, Tian Z-Q. 2009. Surface-enhanced Raman spectroscopy: substrate-related issues. *Anal. Bioanal. Chem.* 394:1729–45
78. Park S, Yang P, Corredor P, Weaver MJ. 2002. Transition metal-coated nanoparticle films: vibrational characterization with surface-enhanced Raman scattering. *J. Am. Chem. Soc.* 124:2428–29

79. Jiang Y-X, Li J-F, Wu D-Y, Yang Z-L, Ren B, et al. 2007. Characterization of surface water on Au core Pt-group metal shell nanoparticles coated electrodes by surface-enhanced Raman spectroscopy. *Chem. Commun.* 2007:4608–10
80. Wu D-Y, Li J-F, Ren B, Tian Z-Q. 2008. Electrochemical surface-enhanced Raman spectroscopy of nanostructures. *Chem. Soc. Rev.* 37:1025–41
81. Stöckle RM, Suh YD, Deckert V, Zenobi R. 2000. Nanoscale chemical analysis by tip-enhanced Raman spectroscopy. *Chem. Phys. Lett.* 318:131–36
82. Anderson MS. 2000. Locally enhanced Raman spectroscopy with an atomic force microscope. *Appl. Phys. Lett.* 76:3130–32
83. Hayazawa N, Inouye Y, Sekkat Z, Kawata S. 2000. Metallized tip amplification of near-field Raman scattering. *Opt. Commun.* 183:333–36
84. Pettinger B, Picardi G, Schuster R, Ertl G. 2000. Surface enhanced Raman spectroscopy: towards single molecule spectroscopy. *Electrochemistry* 68:942–49
85. Bailo E, Deckert V. 2008. Tip-enhanced Raman scattering. *Chem. Soc. Rev.* 37:921–30
86. Deckert V, ed. 2009. Tip-enhanced Raman spectroscopy. *J. Raman Spectrosc.* (*Spec. Iss.*) 40:1335–457
87. Pettinger B, Ren B, Picardi G, Schuster R, Ertl G. 2004. Nanoscale probing of adsorbed species by tip-enhanced Raman spectroscopy. *Phys. Rev. Lett.* 92:096101
88. Ren B, Picardi G, Pettinger B, Schuster R, Ertl G. 2005. Tip-enhanced Raman spectroscopy of benzenethiol adsorbed on Au and Pt single-crystal surfaces. *Angew. Chem. Int. Ed.* 44:139–42
89. Wang X, Liu Z, Zhuang M-D, Zhang H-M, Wang X, et al. 2007. Tip-enhanced Raman spectroscopy for investigating adsorbed species on a single-crystal surface using electrochemically prepared Au tips. *Appl. Phys. Lett.* 91:101105
90. Liu Z, Wang X, Dai K, Jin S, Zeng Z-C, et al. 2009. Tip-enhanced Raman spectroscopy for investigating adsorbed nonresonant molecules on single-crystal surfaces: tip regeneration, probe molecule, and enhancement effect. *J. Raman Spectrosc.* 40:1400–6
91. Schmid T, Yeo B-S, Leong G, Stadler J, Zenobi R. 2009. Performing tip-enhanced Raman spectroscopy in liquids. *J. Raman Spectrosc.* 40:1392–99
92. Taflove A, Hagness SC. 2005. *Computational Electrodynamics: The Finite-Difference Time-Domain Method*. Norwood, MA: Artech. 3rd ed.
93. Frens G. 1973. Controlled nucleation for the regulation of the particle size in monodisperse gold suspensions. *Nat. Phys. Sci.* 241:20–22
94. Liz-Marzán LM, Giersig M, Mulvaney P. 1996. Synthesis of nanosized gold-silica core-shell particles. *Langmuir* 12:4329–35
95. Corrigan DS, Foley JK, Gao P, Pons S, Weaver MJ. 1985. Comparisons between surface-enhanced Raman and surface infrared spectroscopies for strongly perturbed adsorbates: thiocyanate at gold electrodes. *Langmuir* 1:616–20
96. Gao P, Weaver MJ. 1986. Metal-adsorbate vibrational frequencies as a probe of surface bonding: halides and pseudohalides at gold electrodes. *J. Phys. Chem.* 90:4057–63
97. Li X, Gewirth AA. 2003. Potential-dependent reorientation of thiocyanate on Au electrodes. *J. Am. Chem. Soc.* 125:11674–83
98. Rodriguez JA, Goodman DW. 1992. The nature of the metal-metal bond in bimetallic surfaces. *Science* 257:897–903
99. Zou S, Weaver MJ. 1998. Surface-enhanced Raman scattering on uniform transition-metal films: toward a versatile adsorbate vibrational strategy for solid-nonvacuum interfaces? *Anal. Chem.* 70:2387–95
100. Weast RC, Astle MJ, eds. 1982. *CRC Handbook of Chemistry and Physics*. Boca Raton: CRC. 63rd ed.
101. Bus E, van Bokhoven JA. 2007. Electronic and geometric structures of supported platinum, gold, and platinum-gold catalysts. *J. Phys. Chem. C* 111:9761–68
102. Tian Z-Q, Ren B, Chen Y-X, Zou S-Z, Mao B-W. 1996. Probing electrode/electrolyte interfacial structure in the potential region of hydrogen evolution by Raman spectroscopy. *J. Chem. Soc. Faraday Trans.* 92:3829–38
103. Li J-F, Anema JR, Yu Y-C, Yang Z-L, Huang Y-F, et al. 2011. Core-shell nanoparticle based SERS from hydrogen adsorbed on a rhodium(111) electrode. *Chem. Commun.* 47:2023–25

104. Nikoobakht B, El-Sayed MA. 2003. Preparation and growth mechanism of gold nanorods (NRs) using seed-mediated growth method. *Chem. Mater.* 15:1957–62
105. Schulte F, Mäder J, Kroh LW, Panne U, Kneipp J. 2009. Characterization of pollen carotenoids with in situ and high-performance thin-layer chromatography supported resonant Raman spectroscopy. *Anal. Chem.* 81:8426–33
106. Lee D, Lee S, Seong GH, Choo J, Lee EK, et al. 2006. Quantitative analysis of methyl parathion pesticides in a polydimethylsiloxane microfluidic channel using confocal surface-enhanced Raman spectroscopy. *Appl. Spectrosc.* 60:373–77

Annual Review of
Analytical Chemistry

Volume 4, 2011

# Contents

**Indexes**



**Errata**

An online log of corrections to the *Annual Review of Analytical Chemistry* articles may be found at http://arjournals.annualreviews.org/errata/anchem